

Temporal dynamics of viral fitness and the adaptive immune response in HCV infection

Reviewed Preprint

v1 • November 13, 2024

Not revised

Melanie R Walker, Preston Leung, Elizabeth Keoshkerian, Mehdi R Pirozian, Andrew R Lloyd, Fabio Luciani , Rowena A Bull 

The Kirby Institute Viral Immunology Systems Program, Faculty of Medicine, The University of New South Wales, Sydney, Australia • School of Biomedical Sciences Viral Immunology Systems Program, Faculty of Medicine, The University of New South Wales, Sydney, Australia

 https://en.wikipedia.org/wiki/Open_access

 Copyright information

eLife Assessment

The authors examined the evolution of hepatitis C virus (HCV) in a cohort of 14 subjects with recent HCV infections. By using computational methods, they showed that viral fitness declines as the virus mutates to escape the immune response and can rebound later in infection as HCV accumulates additional mutations. The study contributes to an **important** aspect of viral evolution. The combination of approaches is highly **compelling**; however, some aspects of the manuscript are **incomplete** and would greatly benefit from additional revision, mainly to increase their clarity.

<https://doi.org/10.7554/eLife.102232.1.sa2>

Abstract

Numerous studies have shown that viral variants that elude the host immune response may incur a fitness expense, diminishing the survival of the viral strain within the host, and the capacity of the variant to survive future transmission events. Furthermore, co-occurring mutations outside the epitope regions targeted by the immune response may increase or decrease the likelihood of survival of the variant (known as epistasis). Analysis of viral fitness and epistasis over the non-structural protein regions is lacking for hepatitis C virus (HCV). Here, using a rare cohort of subjects very recently infected with HCV, we build upon our prior investigations by integrating mathematical modelling and experimental data to examine the interplay between the evolving transmitted/founder (T/F) viruses, the adaptive immune response, viral fitness, and co-occurring mutations. We show that viral fitness decreases during the first 90 days post-infection (DPI) associated with the magnitude of CD8⁺ T-cell responses and the initial level of diversification. Thereafter, viral fitness rebounds in a complex pattern of evolution characterized by multiple sets of co-occurring mutations. Finally, we show that an early and strong CD8⁺ T-cell response in the absence of neutralizing antibodies (nAbs) imposes a strong selective force on the T/F virus population, enabling the virus to escape and establish chronic infection. Understanding these dynamics is highly

relevant for HCV vaccine design and supports a vaccine strategy that induces broad immunity targeting both T and B cell responses.

Introduction

Hepatitis C virus (HCV) is a major cause of chronic liver disease globally (1). Following acute infection, approximately 75% of people fail to clear the virus, resulting in chronic hepatitis with progressive fibrosis and ultimately cirrhosis, liver failure, and an increased risk of hepatocellular carcinoma (2–5). Despite the arrival of direct-acting antiviral agents (DAA) with remarkable efficacy, the unresolved financial and health service challenges in ensuring universal DAA access to those infected globally, and likelihood of reinfection in high risk populations, necessitate a prophylactic vaccine as an essential component for the WHO goal of global elimination of HCV infection as a public health threat (6).

Due to a high mutation rate during replication, the HCV genome is highly diverse, being classified into eight major genotypes (genotypes 1 to 8), and 86 subtypes (labeled alphabetically [a, b, c, etc.]) (7, 8). HCV also exists within each infected host as a diverse, rapidly evolving population termed a quasispecies. Nevertheless, transmission of HCV is associated with a strong genetic bottleneck with as few as 1–3 transmitted/founder (T/F) viruses commonly establishing infection in the new host, despite hundreds of individual variants found in the source (9, 10). This is followed by a second genetic bottleneck at ~100 days post infection (DPI), where T/F viruses become undetectable, but are replaced by new variants in those who progress to chronic infection, which carry mutations within B-cell and CD8⁺ T-cell epitopes (10). Indeed, clearance of HCV has been associated with an early onset of T/F-specific neutralizing antibodies (nAbs) (11–14), while early and strong CD8⁺ T-cell responses against the T/F virus have been found to drive the generation of immune escape mutations found within MHC-I restricted epitopes leading to progression to chronic infection (15, 16).

Numerous virological studies have shown that viral variants that elude the host immune response might incur a fitness expense, diminishing the survival of the viral strain, and the reducing the capacity of the variant to survive future transmission events as the variants mutate away from the T/F virus (17, 18). In HCV, the structural envelope proteins, E1 and E2, which are predominantly targeted by B-cell response including neutralizing antibodies (nAbs), have been found to collectively mediate viral fitness (19). This interdependence suggests that mutations in the E1 protein could potentially compensate for fitness deficits, thereby facilitating the virus' ability to evade antibodies that specifically target the E2 protein (19). Furthermore, comparative analyses of E2 fitness in genotype 1a and genotype 1b sequences found that it may be easier for subtype 1b viruses to evade immune responses (20, 21). By contrast, a comprehensive analysis of the non-structural protein regions (NS1, NS2, NS3, NS4A, NS4B, NS5A, NS5B) in mediating viral fitness is lacking. For the scope of this study, a fitness model developed for HIV (22, 23) and modified for HCV (24) was used to estimate the fitness landscape of HCV subtypes. Sequences in clinical databases were used to represent the circulating viral variants with the assumption that commonly observed viral variants denoted higher fitness. This model was then used to infer the initial fitness landscape by providing the T/F virus and producing a fitness value. The fitness of the subsequent variants was then described as the relative fitness in comparison to the T/F virus, over the course of an infection.

Mutations that can incur a fitness expense can typically be alleviated or compensated by other mutations, making certain combinations of mutations beneficial (25). These co-occurring mutations can arise outside of the epitope regions and facilitate their compensatory effects, thus increasing the likelihood of survival of the variant (26). This phenomenon is called positive epistasis. However, epistasis may also be negative if a combination of mutations provides a smaller fitness gain than anticipated based on the additive effects of the individual mutations.

Nevertheless, epistatic interactions in HCV have not been studied over acute and chronic phase sequences to infer HCV evolution over the course of the infection. Understanding viral fitness and epistatic interactions in HCV is critical in anticipating future substitutions that are antigenically significant, thus aiding in not only mapping the potential landscape of evolution, but also an improved strategic approach for the selection of potent vaccine strains.

Previously, we longitudinally deep sequenced HCV in 14 individuals, who were recently infected with HCV, to identify the T/F virus and the evolving quasispecies during the infection (15, 16). We identified Human Leucocyte Antigen class I (HLA-I) epitopes from the T/F viruses and the mutated variants. Experimental testing using IFN- γ ELISpot revealed that a strong CD8⁺ T-cell response was linked to rapid immune evasion (15, 16). Here, we build upon our prior investigations by integrating mathematical models and experimental data to examine the interplay between evolving T/F viruses, the adaptive immune response, viral fitness, and co-occurring mutations.

Results

Prediction, generation, and validation of HLA class I-restricted epitopes

A total of 14 subjects with primary HCV infection followed from pre-seroconversion until infection outcome were included in this study (Table 1). The first available viremic sample was collected at a median of 68 days post infection (DPI) (range 2 – 337 DPI). Of the 14 subjects included in this study, 8 subjects naturally cleared the infection (termed here clearers) and 6 subjects progressed to chronic infection (termed here chronic progressors). The median time to natural clearance was 163 DPI (range 69–357). Next generation sequencing (NGS) data were available for eight viremic time points from these subjects to study HCV RNA populations in depth. The T/F viruses were estimated from the distribution of variants at the earliest sampling time point as previously described (10, 11, 15). Thirteen of the 14 subjects had a single T/F virus, with only subject 300023 having two T/F viruses identified, as previously published (10, 11, 15). T/F genomes were utilized to predict HLA-I epitopes from the T/F viruses and the mutated variants (16). These epitopes were tested and validated for IFN- γ ELISPOT (Figure S1) (16).

To examine the role of CD8⁺ T-cell responses in driving viral evolution, longitudinal deep sequenced data was analyzed for fixation events as previously described (16). For those subjects who ultimately spontaneously cleared HCV infection, there were no non-synonymous fixation mutations (defined as having frequency of occurrence greater than or equal to 70% in the sequencing data) occurring within epitope regions (Table S1). Therefore, subjects who cleared infection were not included for further analysis of viral fitness and immune escape throughout this manuscript. From the 6 subjects who developed chronic infection, non-synonymous fixation mutations occurring within epitope regions were observed and peptide epitopes were selected (Table S2). A total of 494 out of 10945 (4.51%) potential epitopes across the six chronic subjects (45 - 100 epitopes per subject) were selected and tested for IFN- γ ELISPOT (Table S2, Figure S1). Of those selected for testing, 30 (6.68%) epitopes induced positive responses in the IFN- γ ELISPOT, and of these, 14 epitopes showed evidence of escape (as indicated by reduced recognition in the IFN- γ ELISPOT assay) (Figure 1, Table S2, Figure S1).

The location of these 14 epitopes associated with escape were mostly within the non-structural regions of the HCV genome, with 7 (50%) epitopes identified in NS3 region, 3 (21.4%) in NS5B and 2 (14.3%) in NS2. One (7%) epitope was identified in the Core region and one (7%) in E2 which were both found in subject 300256 (Table 2). Single fixation events were observed in the majority of these epitopes, with the exception of two epitopes (in subjects HOKD0485FX and 300256) where two fixation events occurred (Table 2).

Table 1.

Subject characteristics and time point analysis.

Subject ID ^a	Age	Sex	Disease outcome	GT ^b	HLA-A		HLA-B		First sampling point (DPI) ^c	Time to clearance	Initial viral load	No. samples sequenced ^d	No. T/F ^e viruses
300023	22	M	Chronic	1a	02:01	02:01	44:02	57:01	36	-	19234348	6	2
300240	21	M	Chronic	3a	02:01	02:01	15:01	57:01	44	-	54887	5	1
300256	31	M	Chronic	1a	03:01	24:02	07:02	35:01	44	-	34149824	5	1
HOKD0485FX	26	F	Chronic	1b	01:01	30:01	08:01	13:02	30	-	733849	8	1
THDS1086MX	25	M	Chronic	1a	02:01	32:01	14:02	27:05	16	-	235662	6	1
THGS0684MX	28	M	Chronic	1a	02:01	32:01	27:02	40:01	2	-	140200	5	1
300360	29	M	Clearer	3a	68:02	32:01	14:02	40:01	30	178	5648631	3	1
300277	25	M	Clearer	3a	02:01	11:01	44:02	44:02	39	69	5482503	3	1
MCRLO786FX	25	F	Clearer	1a	01:01	29:02	44:02	44:02	80	115	1846	1	1
400087	32	F	Clearer	1b	24:02	30:04	14:02	15:06	45	139	13118082	2	1
300364	29	M	Clearer	1a	01:01	03:01	07:02	57:01	337	352	1932	1	1
300231	22	M	Clearer	3a	01:01	01:01	07:02	57:01	6	148	2242163	1	1
300089	26	M	Clearer	1b	01:01	30:01	07:02	57:01	181	357	70737	1	1
300164	22	F	Clearer	3a	24:02	32:01	07:02	40:01	71	204	684028	1	1

^aIdentification, ^bGenotype, ^cDays post infection, ^dNext generation sequencing, ^eTransmitted/Founder

Figure 1.

IFN- γ response and the relationship between viral diversity and the rate of immune escape in subjects chronically infected with HCV.

IFN- γ ELISpot values (SFU/million, right y-axis) and viral load (IU/mL, left y-axis) measured in subjects A. 300256, B. THDS1086MX and C. THGS0684MX for epitope-specific CD8+ T cell responses (see key). Subjects HOKD0485FX, 300023 and 300240 have been shown previously (10, 16). Escape variants are shown with a clear symbol of the original epitope found in the transmitted/founder (see key). D. Plot of average Shannon entropy (SE) against the rate of escape for each epitope in each protein region per subject. Plots of average SE against average IFN- γ ELISPOT response at >90DPI (purple) (E.) and <90DPI (green) (F.) are also shown. P values (P) and Pearson's correlation coefficient (R) are shown in the top left corner of each panel.

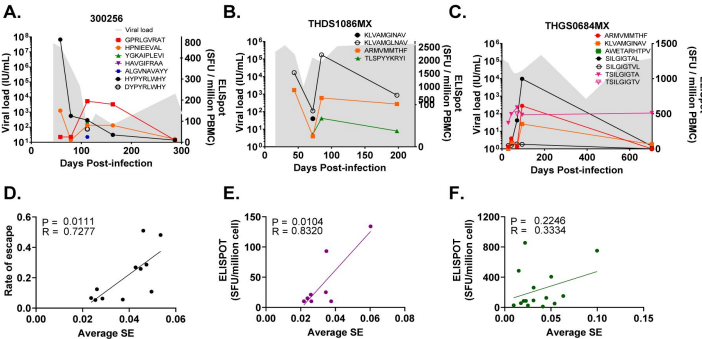


Table 2.

Epitopes and escape rate of epitopes from chronic progressors with fixation events where positive IFN- γ ELISPOT response was detected on the T/F virus.

Subject ID	GT	Epitope (MT) ^{a,b}	Epitope (WT) ^b	Start aa	End aa	Region	ELIS POT ^c	DPI ^d	Matching Subject Allele	Predicted Rank (WT)	Rank Change	Epsilon Estimate ^e	P-value	Fitness Estimated
300023	1a	RAEAHLHAW	RAEAQLHAW	852	860	NS2	91	60	HLA-B*57:01	0.3	0	0.0625	0.0001	Yes
		NSKRTPMGF	KSKRTPMGF	2629	2637	NS5B	484	60	HLA-B*57:01	0.45	-2.2	0.1243	0.0036	Yes
300240	3a	RAQALPPSW	RAQA ^P PPSW	1602	1610	NS3	55	44	HLA-B*57:01	0.2	0	0.1025	0.0236	Yes
		RLGPVQNEI	RLGPVQNE ^V	1633	1641	NS3	300	71	HLA-A*02:01	1.6	-2.1	0.0303	0.0001	Yes
300256	1a	DYPYRLWHY	HYPYRLWHY	610	618	E2	750	58	HLA-A*24:02	1.45	-0.5	0.4813	0.0242	N/A
		GP ^{KM} GVRAT	GPRLGVRAT	41	49	Core	25	58	HLA-B*07:02	0.4	-1.4	0.0532	0.0413	N/A
		HPSIEEVAL	HPNIEEVAL	1359	1367	NS3	150	58	HLA-B*35:01	0.5	0	0.0565	0.0001	Yes
HOKD048 5FX	1b	HSRRKCDEL	HSKKKCDEL	1395	1403	NS3	55	79	HLA-B*08:01	3.3	0.5	0.2685	0.9720	Yes
THDS1086 MX	1a	KLVAMGLNAV	KLVAMGINAV	1406	1415	NS3	85	72	HLA-A*02:01	0.75	0.5	0.5098	0.0005	Yes
		TLSPYYKRHI	TLSPYYKRYI	830	839	NS2	30	72	HLA-A*02:01	3.35	-6.05	0.0689	0.0003	Yes
		VRMVMMTHF	ARMVMMTHF	2841	2849	NS5B	25	72	HLA-B*27:05	0.2	-0.1	0.2582	0.0034	Yes
THGS0684 MX	1a	TSILGIGTV	TSILGIGTA	1324	1332	NS3	230	58	HLA-A*02:01	32	17	0.2861	0.0145	Yes
		SILGIGTVL	SILGIGTAL	1325	1333	NS3	405	58	HLA-A*02:01	5.6	-1.2	0.2861	0.0145	Yes
		AWETARYTPV	AWETARHTPV	2816	2825	NS5B	50	58	HLA-A*02:01	36.5	3.5	0.1082	0.0484	Yes

^a Final most dominant escape variant is shown (i.e. frequency of occurrence >70%)

^b red shows the positions which undergo amino acid change

^c IFN- γ ELISPOT test of autologous PBMC measured in SFU per million PBMC against wild type epitope at earliest sample time point with a positive assay (shown in DPI column). WT - Wild Type and MT - Mutant (Mutant epitopes are sourced from the final available deep sequenced data point).

^d Days post infection ^e The epsilon estimate is the rate of escape given in per day.

CD8+ T-cell responses contribute to the diversification of the viral population

In these same subjects, we previously found that high magnitude of IFN- γ responses were associated with rapid viral immune escape (16). To expand on this data and determine whether viral diversity correlated with the rate of immune escape, Shannon entropy (SE) was calculated (10) across each protein region at the preceding time points to those identified to have fixation in T-cell targeted epitopes, and tested (Table 2) against the rate of escape (ϵ) estimated from the distribution of viral mutations in the NGS data. A significant positive correlation was found between SE and the rate of escape (Pearson's correlation = 0.73, p-value = 0.01), indicating the higher diversity was associated with the occurrence of immune escape (Figure 1D).

To determine whether CD8+ T-cell pressure was driving genomic diversification before and after the genetic bottleneck, the average IFN- γ ELISPOT response within each subject was calculated across multiple epitopes in the same protein region at each time point. This data was then correlated with global SE at two periods, <90DPI and >90DPI. At >90DPI a significant positive correlation was found (Pearson's correlation = 0.83, p-value = 0.01, Figure 1E), indicating that a stronger IFN- γ ELISPOT response was associated with higher diversity following the second genetic bottleneck. Interestingly, this relationship was not evident when examining time points at <90DPI (Pearson's correlation = 0.33, p-value = 0.23, Figure 1F). When considering both pre- and post-90DPI periods, diversity appeared to be influenced by distinct selective pressures where the CD8+ T-cell response plays a significant role in shaping viral population diversity, along with the emergence of epitope escape variants at >90DPI.

Viral fitness decreases during the first 90DPI and is associated with the magnitude of CD8+ T-cell responses and the initial level of diversification

To understand how CD8+ T-cell responses influence the evolution of viral fitness in the acute phase of infection and how the viral population adapts to the host, a quantitative analysis of viral fitness in viral haplotypes on longitudinal samples was performed. We utilized a fitness model initially developed for HIV and adapted for HCV to estimate the fitness landscape of various HCV subtypes. This model was then applied to infer the initial fitness landscape by providing the T/F virus, which generated a fitness value. The fitness of subsequent variants was calculated as relative fitness compared to the T/F virus over the course of the infection. Specifically, fitness of the viral population was estimated for the six chronic progressors (Table 2) in regions NS2, NS3 and NS5B and for each epitope, the population average relative fitness of the viral population over the course of infection was measured (Table 3, Table 4, Table S3 – Table S6).

In general, in the six subjects who progressed to chronic infection, there was a decrease in average relative fitness in the period of <90DPI with respect to the T/F virus (Figure 2). This was with the exception of subject 300023 which can be explained by the presence of two T/F viruses (Figure 2A) where the observed mutations responsible for the increase in viral fitness were present in the genome of the second T/F virus detected at 44DPI carrying substitutions H2750Q and T2917A (Table S3, Figure S2, Figure 2A) (10, 11).

To understand the observed reduction in viral fitness within the first 90DPI, a statistical analysis was performed to examine the relationship between population fitness and immune escape (ϵ), IFN- γ ELISPOT responses and SE values (Figure 3). In the <90DPI period, a significant positive correlation (Pearson's correlation = 0.84, p-value = 0.0004) was identified between population average relative fitness and IFN- γ ELISPOT response (Figure 3A). A significant negative

Table 3

Co-occurring mutations, epitope escape mutants and the associated frequency of occurrence, and relative fitness of NS3 region of subject THDS1086MX.

Viral Load		Frequency	Relative Fitness	1406KLVAMGLNAV ₁₄₁₅	
Time	(IU/ml)			Mutations	Co-occurring Mutations*
16DPI	235662	61.70%	1.000		
		18.10%	1.000		
		6.00%	1.000		
		4.80%	0.364	V1408A	
		4.60%	1.000		
		1.70%	1.000		
		1.60%	0.364	V1408A	
		1.40%	1.000		
72DPI	176550	48.50%	0.453		H1115T
		24.70%	0.453		H1115T
		6.20%	0.453		H1115T
		6.20%	0.453		H1115T
		3.70%	0.084		H1115T C1318Y
		3.60%	0.453		H1115T
		3.30%	0.453		H1115T
		2.10%	0.084		H1115T
109DPI	108737	1.80%	0.069		H1115T C1318Y V1458A
		35.80%	0.223	I1412V	H1115S R1118H
		19.10%	0.384	I1412L	H1115S
		8.60%	0.910	I1412L	V1112A H1115S
		7.70%	0.360	I1412L	V1112I H1115S
		6.30%	0.061	I1412L	H1115G
		5.70%	0.247	I1412L	H1115T
		3.70%	0.657	I1412L	V1112T H1115S
		2.60%	0.145	I1412L	V1112A H1115T
		2.30%	0.062	I1412L	V1112I H1115G
		2.20%	0.229	I1412L	V1112I H1115T
		2.20%	0.573	I1412L	V1112A H1115T
		2.10%	0.624	I1412V	H1115S
		1.80%	0.309	I1412L	H1115A
198DPI	681389	73.60%	0.360	I1412L	V1112I H1115S
		12.60%	2.149	I1412L**	V1112I H1115S A1593V
		4.70%	1.683	A1409T	V1112P H1115S
		2.90%	0.360	I1412L	V1112I H1115S
		1.80%	0.360	I1412L	V1112I H1115S
		1.70%	1.683	A1409T	V1112P H1115S
		1.60%	0.066	I1412L	V1112I H1115S M1268I
		1.20%	0.360	I1412L	V1112I H1115S

****Bold** - indicate escape variants with fitness estimate ≥ 1 .

*Only non-synonymous mutations are shown.

Table 4

Co-occurring mutations, epitope escape mutants and the associated frequency of occurrence and relative fitness of NS3 region of subject THGS0684MX.

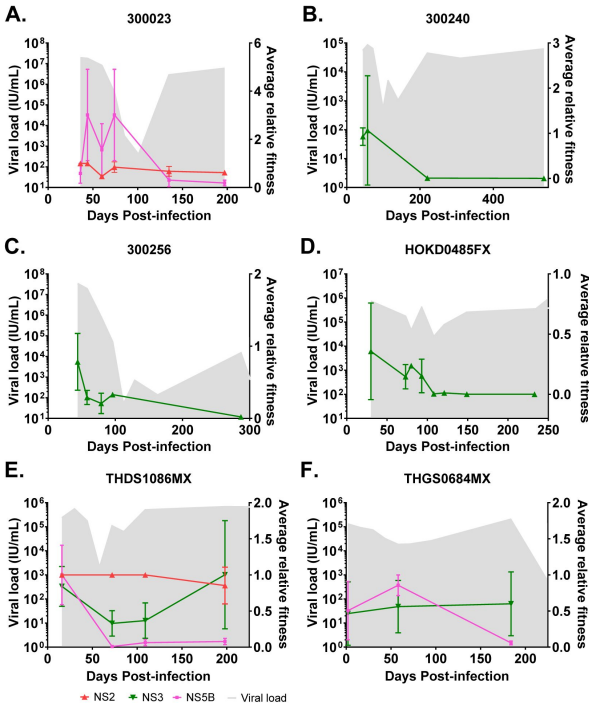
Time	Viral Load (IU/ml)	Frequency	Relative Fitness	¹³²⁵ SILGIGTAL ¹³³³ Mutations	Co-occurring Mutations*
2DPI	140200	87.9%	1.000		
		4.8%	0.148		G1076W
		3.2%	1.000		
		3%	0.155		G1076R
		1.1%	0.022		G1076W Y1521C
58DPI	19932	74.2%	1.000		
		10.8%	1.000		
		8.4%	0.322		
		5.5%	0.162		M1649T
		1%	0.322		S1289G
184DPI	221964	90.9%	1.042	A1332V**	P1496S
		9.1%	0.157	A1332V	D1316G P1496S

*Only non-synonymous mutations are shown.
** **Bold** - indicate escape variants with fitness estimate ≥ 1.

Figure 2.

Longitudinal fitness plots of subjects chronically infected with HCV.

Longitudinal fitness plots of subjects A. 300023, B. 300240, C. 300256, D. HOKD0485FX, E. THDS1086MX and F. THGS0684MX are shown. Grey shade indicates viral load and is measured in IU/ml on the right y-axis. Coloured lines indicate population average relative fitness estimate (right y-axis) for protein regions (see key). Vertical bars indicate standard deviation of population average relative fitness.



correlation between fitness estimate and SE (Pearson's correlation = -0.48, p-value = 0.01) was also identified in the <90DPI period (**Figure 3B**). No significant correlation was observed between ϵ and fitness estimates at <90 DPI (Pearson's correlation = 0.34, p-value = 0.32) (**Figure 3C**).

Similar to the analysis performed at <90DPI, correlation tests were performed to understand the change in fitness at >90DPI (**Figure 3**). No significant correlations were observed between the average relative fitness estimates and IFN- γ ELISPOT (Pearson's correlation = 0.55, p-value = 0.25, **Figure 3D**), SE (Pearson's correlation = 0.26, p-value = 0.26, **Figure 3E**) and ϵ (Pearson's correlation = 0.39, p-value = 0.31, **Figure 3F**).

Overall, these results suggest that in the early phase when the T/F virus was the major variant, a fit viral population was targeted by a strong CD8 $^{+}$ T-cell response. Mutations away from the T/F virus then reduced fitness. Insignificant correlations observed in >90DPI also confirmed that once the chronic phase population had adapted against host immune response, immune pressure showed less impact on viral population fitness and diversity when compared to <90DPI.

Viral fitness rebounds with co-occurring mutations after the second genetic bottleneck at >90DPI

After the second genetic bottleneck at >90DPI, when viral load begins to rise, the distribution of relative fitness continued to decrease in most genomic regions analyzed for all six chronic progressors (**Figure 2**). However, THDS1086MX and THGS0684MX showed a contrasting pattern where the relative fitness measured for the NS3 region exceeded the fitness measured for the T/F virus while the relative fitness decreased for the viral variants in comparison to the fitness of the T/F virus in the NS5B region (**Figure 2E-F**). Of note, THDS1086MX and THGS0684MX are purported to be recipients from the same donor and share an identical consensus sequence at <16DPI (11, 27). Furthermore, the pair carry the same HLA-A alleles but different HLA-B alleles (**Table 1**). We wanted to explore the NS3 regions of THDS1086MX and THGS0684MX to further understand the specific mutations contributing to their relative fitness rebound and to elucidate the mechanisms driving viral evolution and adaptation in these individuals.

Further analysis revealed a complex pattern of evolution characterized by multiple sets of co-occurring mutations (**Figure 4**, **Table 3**). In subject THDS1086MX, at 16DPI, viral haplotypes did not carry any co-occurring mutations. However, at 72DPI, a set of three mutations (H1115T, V1458A, C1318Y) were found to be co-occurring within the same viral variant, with its relative fitness estimated to be inferior to the T/F virus (relative fitness = 0.069) (**Table 3**). At 109DPI, multiple combinations of co-occurring mutations were observed. In particular, immune escape mutation $_{1406}\text{KLVAMG(I/L)NAV}_{1415}$ was identified co-occurring with H1115S/G/T and V1112A/I/T. Variants carrying I1412L and H1115S had a relative fitness of at least one third of the T/F virus. The combination of $_{1406}\text{KLVAMG(I/L)NAV}_{1415}$, H1115S and V1112A reached a fitness level nearly equal to the T/F variant (relative fitness of 0.91, **Table 3**). This suggested a 90% restoration of fitness compared to the T/F virus when H1115S and V1112A were combined with the immune escape mutation. Notably, a variant with only $_{1406}\text{KLVAMG(I/L)NAV}_{1415}$ and H1115S exhibited positive epistasis, with a relative fitness of 0.384.

Viral variants with higher fitness than the T/F virus of subject THDS1086MX were observed at 198DPI (**Figure 4**, **Table 3**). One variant carried the epitope mutation $_{1406}\text{KLVAMG(I/L)NAV}_{1415}$ with V1112I, H1115S and an additional mutation A1593V, achieving a relative fitness of 2.14 at a frequency of 12.6%. Another variant with only $_{1406}\text{KLVAMG(I/L)NAV}_{1415}$ V1112I and H1115S, occurring at 73.6%, showed a relative fitness of 0.360. Additionally, a new immune escape mutation, A1409L, co-occurred with V1112P and H1115S at a frequency of 4.70% and exhibited a relative fitness greater than the T/F (relative fitness = 1.68). The combination of $_{1406}\text{KLV(A/T)MGINAV}_{1415}$, V1112P and H1115S did not co-occur with $_{1406}\text{KLVAMG(I/L)NAV}_{1415}$, V1112I and H1115S, indicating a diversifying strategy for host

Figure 3.

The relationship between fitness and the magnitude of the immune response (SE and IFN-γ ELISPOT) and the rate of escape at <90DPI and >90DPI.

The relationship of population fitness against A. average IFN-γ ELISPOT, B. average Shannon entropy (SE) and C. rate of escape at <90DPI (green) were measured by Pearson's correlation. The relationship of population fitness against D. average IFN-γ ELISPOT, E. average Shannon entropy (SE) and F. rate of escape at >90DPI (purple) were also measured by Pearson's correlation. P values (P) and Pearson's correlation coefficient (R) are shown in the top left corner of each panel.

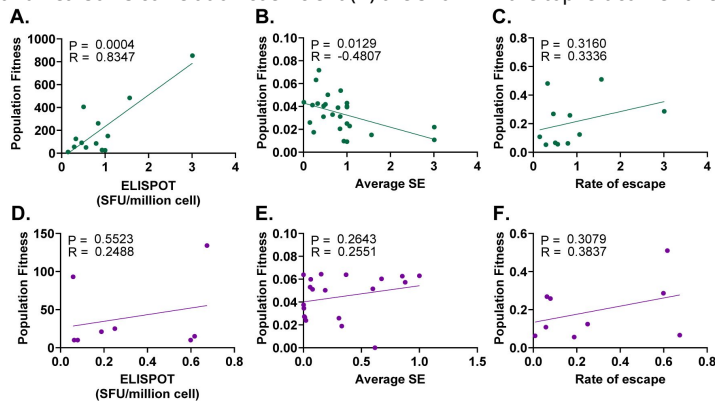
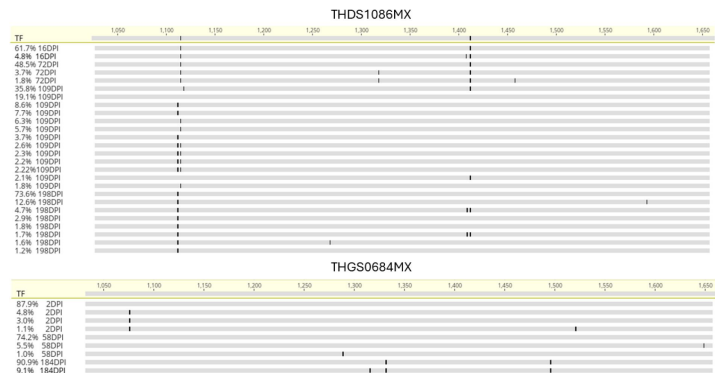


Figure 4.

Longitudinal co-occurring mutations in the NS3 region for subjects THDS1086MX and THGS0684MX.

Highlighter plots (Geneious Prime 2023) derived from longitudinal sequencing from subjects THDS1086MX (top) and THGS0684MX (bottom) indicating co-occurring mutations relative to the transmitted/founder (TF) across the NS3 region. Numbers above highlighter plots denote the genomic amino acid number for the NS3 region. Sequences are labelled by frequency of occurrence (%) and days post infection (DPI). Specific amino acid changes are shown in Table 3 and Table 4.



adaptation. Overall, the combination of I1412L, V1112I and H1115S emerged as the most advantageous mutation combination, enhancing virus fitness, and reaching fixation in the viral population over the course of infection.

For THGS0684MX, co-occurring mutations in the NS3 region occurred in a much simpler fashion (Table 4), where the immune escape mutation $_{1325}\text{SILGIGT(A/V)}_{\text{L1333}}$ achieved a relative fitness of 1.042 when co-occurring with P1496S. The effect of the synergistic mutations was also reflected in the fact that this variant reached 90.9% frequency of occurrence in the viral population at the last sequenced time point of 184DPI (Figure 4, Table 4).

To determine if the increase in estimated fitness was associated with reversion events, namely mutations towards common circulating variants that are assumed to be a more fit HCV strain (generated as previously described (15)). Comparison of the non-synonymous mutations at the final sequence time point in both subjects THDS1086MX and THGS0684MX to the global Genbank genotype 1a consensus sequence were performed. This revealed that V1112P and A1593V (12.6% frequency) in subject THDS1086MX were both reversions toward the worldwide consensus (Figure 4, Table 3). Similarly, for subject THGS0684MX, the mutation A1332Y (90.9% frequency) also reverted to the global consensus strain (Figure 4, Table 4).

These findings suggest rapid adaptation of chronic HCV variants post-strong CD8+ T-cell responses during acute infection, supported by positive epistasis via compensatory mutations post-second genetic bottleneck. Variations between subjects with identical T/F viruses imply a unique fitness restoration strategy for each individual rather than a universal mutation pattern across subjects sharing the same T/F variant.

In chronic progressors, nAbs emerge after CD8+ T-cells and coincide with the rebound of viral fitness

Previously, we have shown that an early nAb response is associated with clearance (11). In those that develop chronic infection, nAb activity is truly delayed and develops towards longitudinal variants after the T/F is cleared (11). Furthermore, we have shown previously (15, 16) that CD8+ T-cell responses impose a strong selective force on the T/F virus population, thus contributing to its extinction and to the rise of the escape variants with the establishment of chronic infection. Here, a comprehensive analysis integrating nAb responses, CD8+ T-cell responses, and viral fitness was performed to elucidate the dynamic interplay between the adaptive immune system and viral evolution and fitness.

All six chronic subjects included in this study had data for nAb responses (11), IFN- γ ELISPOT responses and viral fitness readily available. A subset of three clearer subjects had data for nAb responses (11) and IFN- γ ELISPOT responses (Figure 5 and Figure S3). As mentioned above, viral fitness could not be estimated for clearer subjects due to a lack of non-synonymous fixation mutations occurring within epitope regions.

The timing of the first nAb responses and the IFN- γ ELISPOT response were assessed to elucidate the dynamics of both CD8+ T-cell and nAb responses and their role in clearance or chronic outcomes. In the subset of three clearer subjects (those tested for both nAb responses (11) and IFN- γ ELISPOT responses) no significant difference was found in the timing of nAb and IFN- γ ELISPOT responses, with both responses emerging in all three subjects at <100 DPI (Figure 5A). However, for chronic progressors, IFN- γ ELISPOT responses were first detectable at an average of 48 DPI (range 30 – 80 DPI) whereas nAb responses occurred significantly later, with an average onset of 465 DPI (range 74 – 945 DPI), indicating a notable delay compared to CD8+ T-cell responses ($p = 0.0313$, Wilcoxon matched-pairs signed rank test, Figure 5B).

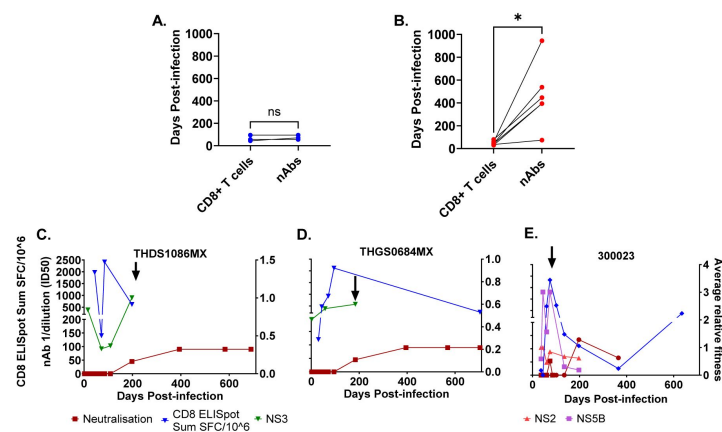


Figure 5.

HCV neutralizing antibody (nAb), CD8+ T cell responses and viral fitness.

The timing (Days post infection) of CD8+ T cell and nAbs are compared for clearer subjects (A) and chronic subjects (B). Statistical significance (Wilcoxon matched-pairs signed rank test) is represented by asterisks ($p < 0.05$ (*)) and non-significance by NS. Panels C - E shows 3 representative subjects who developed chronic HCV infection. The blue line represents the IFN- γ ELISPOT (SFU/million). The maroon line represents HCV nAb ID50 titre with squares representing timepoints tested on autologous virus and circles representing timepoints tested on heterologous virus. Population average relative fitness estimate of regions NS5B (purple), NS3 (green) and NS2 (pink) are shown. Black arrows represent increases in average relative fitness.

Interestingly, in subjects THDS1086MX and THGS0684MX, we observed escape variants with higher relative fitness emerging concurrently with the onset of nAbs at 198 and 184 DPI, respectively (**Figure 5E**, F). Additionally, upon the appearance of nAbs, there was a decline in IFN- γ ELISPOT, while nAb responses remained stable. This suggests a transition from CD8+ T-cell dominant immune responses to nAb dominant immune responses. It's noteworthy that a similar pattern was observed in subject 300023, where an increase in viral fitness coincided with a weak but detectable nAb responses towards the T/F virus at 74 DPI (**Figure 5G**). Nevertheless, nAbs were undetectable at the subsequent timepoint while the IFN- γ ELISPOT response dominated until 200 DPI when nAb responses reappeared and increased along with IFN- γ ELISPOT. This suggests that nAbs were ineffective in controlling the virus in subject 300023 during this period (<100DPI). For the other three subjects, no consistent pattern was observed (**Figure S3**). Specifically, for subjects HOKD0485FX and 300256, nAbs emerged well after viral decline, and there was a lack of CD8+ T-cell data at the positive nAb timepoints, while for subject 300240 both IFN- γ ELISPOT and nAb responses increased after 300DPI.

Together, these results show that an early and strong CD8+ T-cell response in the absence of nAbs imposes a strong selective force on the T/F virus population, enabling the virus to escape and establish chronic infection.

Discussion

Using a rare cohort of very recently infected individuals we report the dynamics of evolution of the viral quasispecies and the role of the host cytotoxic T-cell and nAb responses during the acute phase of primary HCV infection. We show that viral fitness decreases during the first 90DPI associated with the magnitude of CD8+ T-cell responses and the initial level of diversification. Thereafter, viral fitness rebounds in a complex pattern of evolution characterized by multiple sets of co-occurring mutations. Finally, within this cohort of very recently HCV infected individuals we show that an early and strong CD8+ T-cell response in the absence of nAbs imposes a strong selective force on the T/F virus population, enabling the virus to escape and establish chronic infection. Understanding these dynamics is crucial for developing effective vaccines for HCV.

We have previously demonstrated in HCV that a genetic bottleneck occurs in the viral population at around three months post-infection, where the T/F is replaced with new viral variants that dominate infection (10, 15). These new variants carry amino acid changes across the viral genome, including HLA-I restricted epitopes, highlighting that T-cell responses, in the absence of nAbs, play a significant role in driving immune escape. (10, 15, 16, 28, 29). Nevertheless, the majority of studies on HCV CD8+ T-cell responses to date focus only on the epitope and its escape variant without analyzing viral fitness or surrounding mutations which co-occur with the immune escape mutation (30). To understand this process, a quantitative analysis of viral fitness relative to viral haplotypes was conducted using longitudinal samples. We observed a decrease in population average relative fitness in the period of <90DPI with respect to the T/F virus in chronic subjects. The decrease in fitness correlated positively with IFN- γ ELISPOT responses and negatively with SE indicating that CD8+ T-cell responses drove the rapid emergence of immune escape variants, which initially reduced viral fitness.

While a recent study examined mutations in the E2 region, revealing that certain co-occurring mutations led to a loss of E2 function in clearers but a gain in function for chronic progressors (31), the impact of co-occurring mutations in the nonstructural regions on HCV outcomes remains largely unexplored (25, 30, 32, 33). Furthermore, previous studies on HCV have not integrated CD8+ T-cell responses, longitudinal tracking of immune escape mutations, co-occurring mutations, and fitness estimation to analyze HCV evolutionary mechanisms (34). Combining these approaches provides a clearer understanding of HCV evolution by showing how co-occurring mutations impact viral survival over time. We observed that in some subjects,

combinations of mutations could compensate for the negative fitness cost of immune escape, leading to a rebound in viral fitness during infection. This was not observed in all subjects and indicates that each subject's mutation strategy is unique, even when there are shared HLA alleles (such as for subjects THDS1086MX and THGS0684MX).

When analysis of nAb responses, CD8+ T-cell responses, and viral fitness was performed, it was interesting to note the opposite trend with regards to the humoral response in these same subjects. While it remains unclear how T- and B-cell components of the immune system might co-operate to confer protection, the findings of the current study strongly suggest that the absence of nAbs in chronic progressors enables viruses to continue to infect new cells, replicate and mutate. This suggests a synergistic interplay between the B and T-cell arms of the adaptive response targeting the virus and the importance of co-occurrence of these responses. Several studies have alluded to this ([11](#), [15](#), [16](#)) yet to date no study has directly compared B and T-cell responses longitudinally in very recently infected clearers and chronic progressors. Furthermore, in chronic subjects where relative fitness increased after the genetic bottleneck, this increase coincided with the onset of nAbs ([11](#), [31](#)). The fitness model in this study serves as a surrogate for viral fitness, starting with the T/F virus as the baseline and calculating the fitness of subsequent variants relative to this initial measure, enabling us to track fitness changes throughout the infection. Additionally, in these subjects, the appearance of nAbs was associated with a decline in IFN- γ ELISPOT responses, while nAb responses remained stable, suggesting a shift from CD8+ T-cell responses to nAb responses.

In conclusion, this work provides initial insights into how co-evolving mutations contribute to the evolutionary dynamics observed during HCV infection. Furthermore, we show that an early and strong CD8+ T-cell response in the absence of nAbs imposes a strong selective force on the T/F virus population, enabling the virus to escape and establish chronic infection. This could explain the lack of association with a lower incidence of chronic HCV infection compared to placebo observed in the recent Phase I/II trials of the ChAd3-NSmut and MVA-NSmut vaccines, which aimed to induce T cell responses by encoding HCV NS proteins ([35](#)). While much work is still required to be able to fully understand the factors contributing to the overall dynamics of HCV infections, this work has the potential to inform design of the next generation of vaccines.

Methods

Subjects and samples

Samples were available from two prospective cohorts of HCV-seronegative and aviremic, high-risk, individuals enrolled in the Hepatitis C Incidence and Transmission Studies (HITS) in prisons (HITS-p), or in the general community (HITS-c), as previously described ([11](#), [27](#), [36](#), [37](#)). Risk behavior data and blood samples were collected every six months to screen for HCV RNA positivity and seroconversion. Participants identified as early incident cases were enrolled into a sub-cohort called HITS-incident (HITS-i) upon detection of new onset viremia without antibodies, as described previously ([11](#)). These subjects were then frequently sampled for 12 weeks before being offered antiviral treatment at 24 weeks, allowing for the classification of outcomes as either natural clearance or chronic infection. The date of infection was estimated by subtracting the average HCV pre-seroconversion window period, which has been estimated at 51 days from the midpoint between last seronegative and first seropositive time points as previously described ([10](#), [11](#), [38](#), [39](#)). Molecular HLA typing was performed at the Institute of Immunology and Infectious Diseases in Perth, Australia, using second-generation sequencing of HLA-A/B/C genes as previously described ([40](#)). 14 subjects with stored peripheral blood mononuclear cells (PBMCs) were selected from the HITS-i cohort. This group included 8 subjects with acute HCV infection and 6 subjects who developed chronic infection.

PBMCs were isolated from peripheral blood via density-based centrifugation, and resuspended in RPMI (Sigma-Aldrich, MO) supplemented with penicillin, streptomycin, l-glutamine, and fetal bovine serum at 1×10^6 cells/mL.

Viral sequencing and identification of T/Fs and longitudinal variants

Near full length HCV genome amplification and sequencing datasets of the full-length viral genomes at multiple timepoint have been published previously (10, 11, 15, 16, 41, 42). Briefly, near full length HCV genome amplification was performed using an nRT-PCR (41). Illumina (MiSeq Benchtop sequence, San Diego, USA) sequencing were performed on amplicons from longitudinal time points of the 14 subjects (11, 16, 41). A bioinformatics pipeline was used to clean and align reads generated from next generation sequencing (NGS) (10, 11, 15). To accurately detect single nucleotide polymorphisms (SNPs) from the aligned and cleaned sequences, analysis was performed to correct for random technical errors using the software ShoRAH, LoFreq and Geneious (11, 43, 44). Haplotypes were reconstructed from NGS data across the full genome using ShoRAH and QuasiRecomb (43, 45). As described previously (10, 11, 15, 16), to determine T/Fs, a statistical model, Poisson fitter, as well as phylogenetic analysis was applied to haplotypes from the first available viremic timepoint but prior to the first HCV antibodies (seroconversion) detection, for each subject to determine the T/F (46). Shannon Entropy was determined from the NGS data as previously described (10).

CD8+ T-cell epitope selection

For each of the 14 subjects, non-synonymous fixation events (>70% frequency in the viral population) from the last time point sequenced were substituted into the TF sequence, thus generating a modified sequence termed the fixation sequence.

Identification of MHC-Class I restricted epitopes (9 to 10 amino acids) was performed by analysis of both HCV/TF and fixation sequences in conjunction with MHC Class I genotyping to predict epitopes and then compared with previous experimentally confirmed epitopes from the Immune Epitope Data Base (IEDB [www.iedb.org]). This resulted in each prediction list containing at least 10,000 epitope predictions.

Due to the large number of epitopes and the lack of available PBMCs, a bioinformatics pipeline, *iedb_tool*, was developed in Python 2.7 to identify a subset of epitopes for further experimental and bioinformatics analyses. This software package is freely available and can be downloaded at: <https://github.com/PrestonLeung/IEDBTool2>. The predicted epitopes generated from IEDB were downloaded in plain text format and parsed into *iedb_predictionParser.py* with options *-lower 100.0* to extract relevant subject information (HLA genotypes, predicted epitope sequence, start and end positions of the epitope sequence). The predicted data set was then used with the experimentally validated epitopes from IEDB. This step generated a categorized list of ranked epitopes for which predicted epitopes and HLA-I typing for each subject were matched with experimentally validated epitopes. An 80% homology threshold was set to facilitate small differences between the autologous epitope sequence and those that were previously reported from the IEDB database.

We prioritized epitopes that matched the HLA allele of the subject and classified these into three categories. Category 1 included epitopes for each subject from which the mutated variant was no longer predicted to be recognized, indicating a potential escape variant. Category 2 included epitopes from those that underwent escape, but the variant was still predicted to be recognized by CD8+ T-cells and category 3 included epitopes that did not mutate during infection. A threshold of 10th percentile ranking or higher was used as a cut off for epitope selection. For categories 2 and 3, we selected a maximum of 10 epitopes due to limitations in PBMC samples. An upper limit of 100 epitopes was set for each subject to account for the total PBMCs available for each time point in

the ELISpot matrix testing approach (see below). If the above criteria gave a total number of epitopes less than 40, then epitopes from categories 2 and 3 were searched with a lowered threshold of 50th percentile ranking or higher to increase the sample size to at least 40. This refined list of ranked epitopes we refer to throughout the manuscript as “potential epitopes”.

IFN- γ ELISPOT validation

Potential epitopes generated above were analyzed using matrix IFN- γ ELISPOT assays as previously described (15, 16). Briefly, peptides were synthesized by Mimotopes Australia and used in autologous CD8⁺ T-cell ELISpot assays in pools of ≤ 5 peptides per well in a matrix format. The peptides were pooled such that any two wells would only have one common peptide and each peptide was tested in at least two separate wells.

As previously described by us (15, 16), PBMC were added to a 96-well ELISpot plate (MAIPS; Millipore, USA) precoated with gamma interferon (IFN- γ) (Mabtech, Sweden) at a concentration of 150,000 cells per well and incubated overnight with peptides (final concentration of 10 μ g/ml). Plates were read and analyzed using an AID plate reader (Autoimmun Diagnostika GmbH, Germany). A peptide/well was concluded to be a positive if it demonstrated an interferon- γ (IFN- γ) response ≥ 25 spot-forming units per million cells (SFU/million) and a negative control count of zero. A confirmation experiment using the IFN- γ ELISpot assay was conducted for individual positive peptides using one peptide per well in a concentration of 200,000 cells per well. At least one well per study subject was allocated as a positive control (anti-CD3 antibody; Mabtech, Sweden), and three wells were used as negative controls. Background was defined as the mean plus 3 standard deviations of the number of spots counted across the three negative controls.

Estimating the rate of CD8⁺ T-cell epitope escape

The estimation of the rate of CD8⁺ T-cell epitope escape was performed as previously described (15, 16). Briefly, the kinetics of CD8⁺ T-cell escape was estimated with a simple population dynamics model (15, 16, 47). The model predicts that the frequency of the escape variant $f(t)$ is: $f(t) = f_0 f_0 + (1 - f_0) e^{-kt}$, where k is the rate of escape and it is assumed that the escape variant is present at a low frequency beyond the range of detection during the initial phase of time (t) at zero, and its frequency is given by f_0 . The escape variant was defined as any observed mutations away from the wild-type sequence that consequently becomes fixed in the population. Therefore, the frequency of the escape variant at individual longitudinal time point was the total frequencies of each epitope carrying the escape mutation regardless of the other amino acid positions. In some cases where the escape variant was not observed in the earlier time points, an estimate of $1/(n+1)$ replaces a frequency of 0, where n is the average coverage of the corresponding time point from the deep sequencing data. This model was used to estimate the rate of escape only in those cases with experimental evidence (ELISpot data generated in this study) of CD8⁺ T-cell-driven immune escape. Estimates were performed in R using non-linear least-squares approach for non-linear models (48).

Estimating survival fitness of viral variants

Estimates of the viral fitness were performed on each viral variant reconstructed by QuasiRecomb as previously described (22–24). Specifically, haplotype reconstruction was performed longitudinally for each subject in a region of approximately 600 amino acids surrounding the

experimentally confirmed CD8+ T-cell epitopes. The fitness landscape inference is obtained by estimating the parameter of a function $E(\vec{z})$ representing the energy of the viral population and with $P(\vec{z})$:

$$P(\vec{z}) = \frac{e^{-E(\vec{z})}}{z},$$

$$E(\vec{z}) = \sum_{i=1}^m h_i(z_i) + \sum_{i=1}^m \sum_{j=i+1}^m J_{ij}(z_i, z_j)$$

where \vec{z} is the peptide sequence of length m such that $\vec{z} = \{z_1, z_2, \dots, z_m\}$ describes individual amino acids in \vec{z} . $P(\vec{z})$ is the prevalence fitness taken under the assumption that the frequently occurring variants represent the fitter strain (i.e. the common circulating virus, in this case the original T/F virus), and this mathematically defined fitness correlate positively to the actual viral fitness $f(\vec{z})$ (22). $E(\vec{z})$ is the ‘energy’ of peptide \vec{z} a pseudo measurement for fitness and z is a normalization factor described in the following equation.

$$z = \sum_{\vec{z} \in \{1,0\}} e^{-E(\vec{z})}$$

The parameter $h_i(z_i)$ is the contribution of energy of the single amino acid at position i of \vec{z} . $J_{ij}(z_i, z_j)$ specifies the energy contribution associated with pairwise interactions between two amino acids in \vec{z} at positions i and j . Under the model assumptions, the association between measurement of energy and fitness estimate showed a negative correlation where minimal $E(\vec{z})$ maximizes the logarithm of the viral fitness $\log(f(\vec{z}))$ (24).

A relative fitness estimate was also calculated for reconstructed haplotypes by normalizing individual fitness estimates with respect to the fitness of the haplotype corresponding to the T/F variant. These values were used to represent the viral fitness of individual haplotypes to infer viral evolution dynamics with respect to the T/F virus.

This analysis was used to quantify the selection exerted by the host cytotoxic T cell response in driving the evolution of the T/F virus. The analysis also showed the role of specific co-evolving mutations and the identification of epistatic interactions that may determine the evolution of viral fitness and the overall success of the infection.

HCVpp production, infection and neutralization

As previously described by us, E1E2 glycoproteins were cloned and co-transfected with MLV gag/pol and luciferase vectors in 293T-cells to produce HCV-pseudo-particles (pp) (11, 49, 50). Briefly, neutralization assays were performed by incubating HCVpp with heat inactivated plasma for one hour at 37 °C. This mixture was applied directly to Huh-7.5 hepatoma cells (Apath, L.L.C, New York, NY, USA), and incubated for 72 hours after which luciferase activity was measured (11). Neutralization of HCVpp was calculated using the formula: % inhibition = $1 - (\text{inhibited activity})/(\text{‘normal’ activity}) \times 100$, after subtraction of negative control (pseudo-particle generated without glycoproteins) RLU, where normal activity is HCVpp incubated with plasma from a healthy donor. The 50% ID50 titer was calculated as the nAb concentration that caused a 50% reduction in RLU for each plasma/HCVpp combination tested in neutralization. All samples were also tested for neutralizing activity on control pseudo-particle VSV-G, to determine that nAbs were HCV E1E2 specific. All data were fitted using non-linear regression plots (GraphPad, Prism).

Data visualization and statistical analysis

Data visualization for CD8⁺ T-cell analyses were performed using ggplot2 package (51 [↗](#)) in R (48 [↗](#)). Visualization of viral fitness estimates and longitudinal neutralization and CD8⁺ T-cell data was performed using GraphPad Prism version 10.0 for Windows, GraphPad Software, La Jolla California USA (www.graphpad.com [↗](#)). As were comparisons of timing of nAb and CD8⁺ T-cell responses where Wilcoxon matched-pairs signed rank tests were performed. Sequence alignments for highlighter plots were performed on the variants generated here using Geneious Prime 2023 (<https://www.geneious.com> [↗](#)).

Ethics statement

Human research ethics approvals were obtained from Human Research Ethics Committees of Justice Health (reference number GEN 31/05), New South Wales Department of Corrective Services (05/0884), and the University of New South Wales (05094, 08081), all located in Sydney, Australia. Written informed consent was obtained from the participants. All methods were performed in accordance with the relevant guidelines and regulations.

Data availability

Single-cell RNA seq data are available on Accession number GSE196330. All the single-cell RNA-seq data are deposited with GSE196330.

Acknowledgements

We would like to acknowledge Gregory R. Hart and Prof. Andrew L. Ferguson for their assistance with the fitness models.

Supporting information

Subject ID	Disease Outcome	Genotype	No. of positive IFN- γ ELISPOT	No. of epitopes underwent escape	Epitope ^a
300360	Clearer	3a	3	0	YLTAYQATV SVIDCNVAV ATDALMTGF
300277	Clearer	3a	6	0	NLPGCSFSI RLWHYPCTV HSNIEEVAL ILAGYGAGV AWETARHTPV WLGNIIMYA
MCRLO786FX	Clearer	1a	2	0	GPRLGVRAT
400087	Clearer	1b	3	0	ATDALMTGF VHYPYRLWHY GAPITYSTY SFSIFLLAL
300364	Clearer	1a	2	0	KSKRTPMGF ATDALMTGF
300231	Clearer	3a	1	0	RAQAPPPSW
400089	Clearer	1b	1	0	GPRLGVRAT
300164	Clearer	3a	1	0	DYPYRLWHY
Total			19	0	

* - Epitope not used due to length criteria being 9-10mer

a - Epitopes with ≥ 25 SFU / million cells in IFN- γ ELISPOT assay

Table S1

Summary of epitope selection and (IFN- γ) ELISPOT assay responses in subjects who cleared infection.

Subject ID	Disease Outcome	Geno type	No. of potential Epitopes	No. of selected Epitopes	No. of positive IFN- γ ELISPOT	No. of epitopes underwent escape	Epitope ^a
300023	Chronic	1a	2213	45	8	2	(K/N)SKRTPMGF RAEA(Q/H)LHAW CINGVCWTV VLSDFKTWL AEVIAPAVQT FAWYLGKGW AELIEANLLW WLGNIIMFA
300240	Chronic	3a	1188	70	3	2	RAQA(P/L)PPSW RLGPVQNE(V/I) VLSDFKTWL
300256	Chronic	1a	3307	98	6	3	(H/D)YPYRLWHY GP(RL/KM)GVRAT HP(N/S)IEEVAL YGKAIPLEVI HAVGIFRAA ALGVNAVAYY
HOKD0485FX	Chronic	1b	734	82	4	2	HS(KK/RR)KCDEL HPVTKYI(M/T)* STNPKPQR(Q/K) VTLTHPVTKY
THDS1086MX	Chronic	1a	2115	99	4	2	KLVAMG(L/I)NAV TLSPYYKR(Y/H)I ARMVMMTHF VRMVMMTHF
THGS0684MX	Chronic	1a	1388	100	5	3	TSILGIGT(A/V) SILGIGT(A/V)L AWETAR(H/Y)TPV KLVAMGINAV ARMVMMTHF
Total			10945	494	30	14	

* - Epitope not used due to length criteria being 9-10mer, a - Epitopes with ≥ 25 SFU / million cells in IFN- γ ELISPOT assay

Table S2

Summary of epitope selection and positive (IFN- γ) ELISPOT assay responses in subjects who developed chronic infection.

Region	Time	Viral Load*	Relative		852RAEAQLHAW ⁸⁶⁰ 2629KSKRTPMGF ²⁶³⁷ Mutations	Co-occurring Mutations**
			Frequency	Fitness		
NS2	36DPI	19234348	30.80%	1.000		
			27.10%	1.000		
			21.80%	1.000		
			20.30%	1.000		
	44DPI	17907338	31.30%	1.000		
			25.70%	1.000		
			23.70%	1.000		
			19.20%	1.000		
'60DPI'	8121396		86.20%	0.462		F921S
			13.80%	0.462		F921S
'74DPI'	397185		27.60%	1.000		
			19.70%	1.000		
			17.20%	1.000		
			12.30%	1.000		
			5.90%	1.000		
			4.20%	1.000		
			3.50%	1.000		
			2.60%	1.000		
			2.40%	0.536		
			1.80%	0.536		
			1.50%	0.536		
			1.10%	0.536		
135DPI	2843176		63.10%	1.000		
			11.90%	0.617	Q856H	
			9.40%	0.599	Q856L	
			8.00%	1.000		
			2.70%	0.358	A853T	
			1.90%	0.599	Q856L	
			1.60%	0.617	Q856H	
			1.30%	0.599	Q856L	
197DPI	5896155		44.50%	0.617	Q856L	
			21.00%	0.617	Q856L	
			13.20%	0.617	Q856L	
			8.20%	0.617	Q856L	
			6.30%	0.617	Q856L	
			4.20%	0.617	Q856L	
			2.60%	0.617	Q856L	
NS5B	36DPI	19234348	65.80%	1.000		
			20.10%	1.000		
			10.90%	0.175		E2866K
			3.10%	0.175		E2866K

Table S3.

Subject 300023 relative fitness estimate, co-occurring mutations and frequency of occurrence for each reconstructed haplotype.

Table S3. (continued)

44DPI	17907338	7.30%	5.647			H2750Q T2917A
		7.00%	1.428			T2917A
		7.00%	3.966			H2750Q
		6.90%	1.000			
		6.90%	5.647			H2750Q T2917A
		6.70%	1.000			
		6.60%	3.966			H2750Q
		6.50%	1.428			T2917A
		6.10%	1.000			
		5.80%	1.428			T2917A
		5.80%	3.966			H2750Q
		5.70%	1.428			T2917A
		5.60%	3.966			H2750Q
		5.40%	5.647			H2750Q T2917A
		5.30%	5.647			H2750Q T2917A
		5.30%	1.000			
60DPI	8121396	83.60%	1.000			
		3.90%	1.000			
		3.80%	1.428			T2917A
		3.60%	1.000			
		3.40%	1.000			
		1.70%	3.966			H2750Q
74DPI	397185	8.90%	1.000			
		8.20%	1.000			T2917A
		8.20%	1.428			
		7.40%	3.966			H2750Q
		6.80%	1.428			T2917A
		6.70%	1.000			
		6.60%	3.966			H2750Q
		6.00%	1.000			
		6.00%	1.428			T2917A
		5.70%	5.647			H2750Q T2917A
		5.50%	3.966			H2750Q
		5.40%	5.647			H2750Q T2917A
		5.00%	1.428			T2917A
		4.90%	5.647			H2750Q T2917A
		4.40%	3.966			H2750Q
		4.20%	5.647			H2750Q T2917A
135DPI	2843176	43.60%	0.337	K2629N		
		21.00%	0.337	K2629N		
		17.20%	0.337	K2629N		
		7.90%	0.337	K2629N		
		3.50%	0.060	K2629N		T2930S
		2.10%	1.000			
		2.00%	0.141	K2629N		
		1.60%	0.060	K2629N		T2930S
197DPI	5896155	1.20%	0.146	K2629N	R2632G	
		97.90%	0.337	K2629N		
		1.00%	0.171	K2629N		R2690K
		1.00%	0.055	K2629N		D2772E

*Viral Load measured in IU/ML.

**Only non-synonymous mutations are shown.

Table S4.

Subject 300240 relative fitness estimate, co-occurring mutations and frequency of occurrence for each reconstructed haplotype.

					1602RAQAPPPSW1610 1633RLGPVQNEV1641			
Region	Time	Viral Load*	Frequency	Relative Fitness	Mutations		Co-occurring Mutations**	
NS3	44DPI	54887	18.50%	1.0000				
			13.20%	1.0000				
			8.40%	1.0000				
			6.00%	1.0000				
			5.60%	1.0000				
			5.10%	1.0000				
			4.80%	1.0000				
			3.80%	1.0000				
			3.30%	1.0000				
			3.20%	0.4132			T1411I	
			3.00%	1.0000				
			2.80%	1.0000				
			2.50%	1.0000				
			2.40%	0.4132			T1411I	
			2.30%	1.0000				
			2.20%	1.0000				
			2.10%	1.0000				
			1.70%	1.0000				
			1.60%	1.0000				
			1.60%	0.4132			T1411I	
			1.60%	1.0000				
			1.60%	1.0000				
			1.40%	1.0000				
			1.40%	1.0000				
57DPI	85473	53.70%	1.0000					
		23.90%	0.4132			T1411I		
		12.60%	3.5094			V1202I		
		6.10%	1.4445			V1202I		
		2.60%	0.0107			A1576G		
		1.10%	0.0045			A1576G		
220DPI	44449	96.60%	0.0107	P1606L			T1509N	
		1.70%	0.0107	P1606L			T1509K	
		1.70%	0.0016	P1606L	R1395G		T1509N	
538DPI	62174	37.30%	0.0031	P1606L	V1641I			
		35.50%	0.0031	P1606L	V1641I			
		12.60%	0.0031	P1606L	V1641I			
		10.60%	0.0031	P1606L	V1641I			
		2.10%	0.0000	P1606L	V1641I			
		1.80%	0.0000	P1606L	V1641I			

*Viral Load measured in IU/ML.

**Only non-synonymous mutations are shown.

Table S5

Subject 300256 relative fitness estimate, co-occurring mutations and frequency of occurrence for each reconstructed haplotype.

Region	Time	Viral Load*	Frequency	Relative Fitness	1359HPNIEEVAL1367 Mutations	Co-occurring Mutations**
NS3	44DPI	34149824	27.20%	1.000		
			8.30%	1.000		
			7.30%	0.151		
			7.10%	1.000		
			6.90%	1.000		
			5.70%	1.000		
			4.40%	1.000		
			4.20%	0.008		V1109I
			3.90%	0.151		
			3.80%	1.000		
			3.70%	0.001		V1109I
			3.60%	1.000		
			3.60%	1.000		
			2.70%	1.000		
			2.60%	1.000		
			2.50%	1.000		
	58DPI	19188762	51.70%	0.330		V1109I
			14.30%	0.330		V1109I
			11.30%	0.330		V1109I
			10.30%	0.330		V1109I
			5.50%	0.049		V1109I M1268V
			3.70%	0.330		V1109I
			3.20%	0.330		V1109I
	79DPI	812622	75.70%	0.330		V1109I
			7.30%	0.330		V1109I
			6.40%	0.330		V1109I
			5.10%	0.330		V1109I
			3.00%	0.050		V1109I Y1249C
			1.40%	0.035		V1109I C1594Y
			1.10%	0.050		V1109I H1272R
96DPI	50774	100.00%	0.330			V1109I
286DPI	14853	73.90%	0.031	N1361S	V1109I	T1408I
		16.40%	0.007	N1361S	V1109I	T1408I M1646T
		3.60%	0.031	N1361S	V1109I	T1408I
		3.60%	0.004	N1361S	V1109I	T1408I
		2.50%	0.031	N1361S	V1109I	T1408I

*Viral Load measured in IU/ML.

**Only non-synonymous mutations are shown.

Region	Time	Viral Load*	Frequency	Relative Fitness	1395 HSKKKCDEL ₁₄₀₃ Mutations	Co-occurring Mutations**
NS3	30DPI	733849	13.10%	1.0000		
			13.00%	0.1509		D1605G
			11.70%	0.1509		C1518F
			9.80%	0.1509		D1605G
			5.10%	0.1509		D1605G
			5.10%	1.0000		
			4.90%	0.1509		C1518F
			4.50%	1.0000		
			4.00%	1.0000		
			3.60%	1.0000		
			2.30%	0.0336		A1230T A1302T
			2.20%	0.0144		S1536P
			2.10%	0.1511		T1286P
			1.60%	0.1199		
			1.60%	0.0350		V1198A I1314M
			1.60%	0.0228		V1198A
			1.40%	0.1509		P1241S A1302T
			1.20%	0.1509		G1233D
	72DPI	175219	66.90%	0.2373	K1398R	
			7.50%	0.2373	K1398R	
			7.20%	0.2373	K1398R	
			6.40%	0.0358	K1398R	G1307E
			3.10%	0.0364	K1398R	S1215F
			2.60%	0.2373	K1398R	
			2.40%	0.0359	K1398R	Y1644C
			2.20%	0.2373	K1398R	
			1.60%	0.0245	K1398R	T1459I
	79DPI	44452	36.70%	0.2373	K1398R	
			23.80%	0.2373	K1398R	
			23.80%	0.2373	K1398R	
			15.70%	0.2373	K1398R	
	93DPI	407392	41.30%	0.3420	K1398R	V1641I
			27.30%	0.0324	K1398R	V1641I A1113T
			11.20%	0.0516	K1398R	V1641I A1085V
			7.40%	0.0049	K1398R	V1641I A1085V A1113T
			3.40%	0.3420	K1398R	V1641I
			2.30%	0.0324	K1398R	V1641I A1113T

Table S6.

Subject HOKD0485FX relative fitness estimate, co-occurring mutations and frequency of occurrence for each reconstructed haplotype.

Table S6. (continued)

		2.10%	0.2373	K1398R			
		1.70%	0.1189	K1398R		V1641I	R1496G
		1.60%	0.3420	K1398R		V1641I	
		1.50%	0.0223	K1398R		V1641I	A1113T
107DPI	24969	100.00%	0.0039	D1401N		V1641I	
121DPI	77723	19.00%	0.0034	K1398R	K1397R	V1641A	
		11.80%	0.0034	K1398R	K1397R	V1641A	
		10.80%	0.0034	K1398R	K1397R	V1641A	
		7.50%	0.0034	K1398R	K1397R	V1641A	
		5.90%	0.0034	K1398R	K1397R		
		4.30%	0.0285	K1398R	K1397R	V1641A	
		4.30%	0.0034	K1398R	K1397R	V1641A	
		4.00%	0.0034	K1398R	K1397R	V1641A	
		3.10%	0.0295	K1398R		V1641A	
		2.90%	0.0148	K1398R	K1397R	V1641A	
		2.60%	0.0005	K1398R	K1397R	V1641A	I1285V
		2.50%	0.0285	K1398R	K1397R		
		2.40%	0.0285	K1398R	K1397R		
		2.30%	0.0073	K1398R	K1397R	V1641T	
		2.00%	0.0034	K1398R	K1397R	V1641A	
		2.00%	0.0034	K1398R	K1397R	V1641A	
		2.00%	0.0295		K1397R	V1641A	
		1.90%	0.0295		K1397R	V1641A	
		1.90%	0.0005	K1398R	K1397R	V1641A	A1405V
		1.80%	0.0148	K1398R		V1641A	
		1.80%	0.0005	K1398R	K1397R	V1641A	I1285V
		1.70%	0.0148	K1398R		V1641A	
		1.70%	0.0073	K1398R	K1397R	V1641T	
149DPI	254245	97.10%	0.0031	K1398R	K1397R	M1646T	
		1.80%	0.0005	K1398R	K1397R	M1646T	A1597T
		1.10%	0.0005	K1398R	K1397R	M1646T	G1489D
233DPI	350658	62.00%	0.0002	K1398R	K1397R	M1646T	
		12.00%	0.0002	K1398R	K1397R	M1646T	
		3.60%	0.0002	K1398R	K1397R	M1646T	A1647T
		3.50%	0.0002	K1398R	K1397R	M1646T	
		3.20%	0.0000	K1398R	K1397R	M1646T	K1162R
		3.10%	0.0002	K1398R	K1397R	M1646T	
		2.70%	0.0015	K1398R	K1397R	M1646T	V1329I
		2.70%	0.0003	K1398R	K1397R	M1646T	V1641I
		2.60%	0.0002	K1398R	K1397R	M1646T	
		2.50%	0.0002	K1398R	K1397R	M1646T	
		2.20%	0.0002	K1398R	K1397R	M1646T	K1088R

*Viral Load measured in IU/ML.
**Only non-synonymous mutations are shown.

Figure S1.

Magnitude of CD8+ T cell responses associated with escape.

CD8+ T cell responses were tested by IFN-γ ELISPOT assays measuring spot-forming unit per million cells (SFU/million cell) of epitopes (vertical axis) across three populations. Horizontal axis from left to right shows the population of epitopes that undergo fixation events in subjects who became chronically infected by HCV (Ch), epitopes that had no mutations and epitopes from subjects that spontaneously cleared HCV infection (CI). Statistical comparisons are Mann-Whitney tests. Scatter plots represent means and standard deviation.

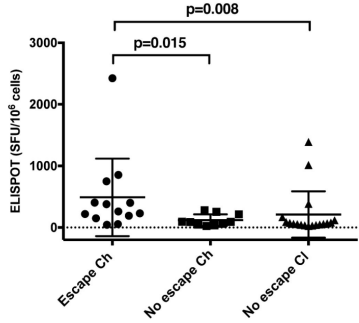


Figure S2.

Phylogenetic analysis of subject 300023 NS5B region.

Diamonds represent haplotypes with blue indicating consensus sequence and green diamonds representing reconstructed haplotypes at 36DPI. Purple diamonds indicate reconstructed haplotypes at 44DPI. The NS5B region shows diversity consistent with the presence of two T/F viruses as previously described by us (10, 11, 15, 16).

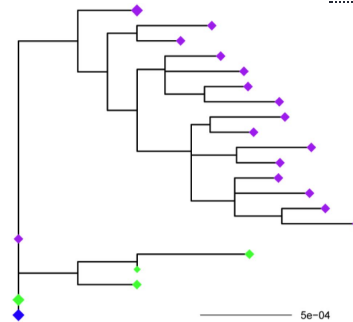
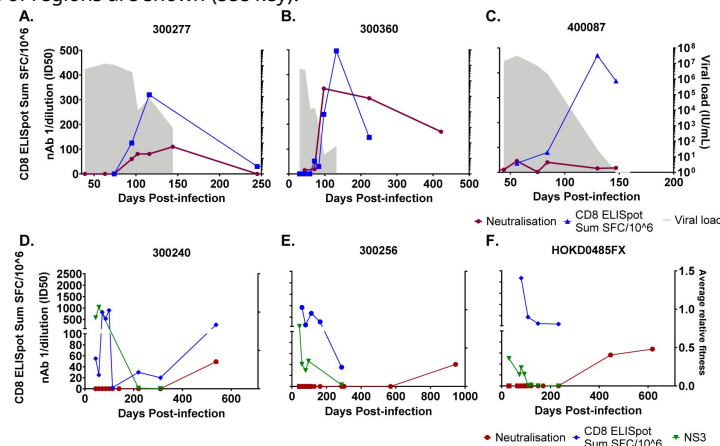


Figure S3.

HCV neutralizing antibody (nAb) and CD8+ T cell responses and viral fitness.

Panels A - C shows 3 subjects who cleared HCV infection and Panels D-F shows three subjects who developed chronic HCV infection. The blue line represents the IFN- γ ELISPOT response (SFU/million). The maroon line represents HCV nAb ID50 titre with squares representing timepoints tested on autologous virus and circles representing timepoints tested on heterologous virus. For panels A-C, the shaded area represents the longitudinal HCV RNA levels (IU/ml). For panels D-F population average relative fitness estimate of regions are shown (see key).



References

1. Lanini S, Easterbrook PJ, Zumla A, Ippolito G (2016) **Hepatitis C: global epidemiology and strategies for control** *Clin Microbiol Infect* **22**:833–8
2. Seeff LB (2002) **Natural history of chronic hepatitis C** *Hepatology* **36**:S35–46
3. Lavanchy D (2009) **The global burden of hepatitis C** *Liver Int* **29**:74–81
4. Micallef JM, Kaldor JM, Dore GJ (2006) **Spontaneous viral clearance following acute hepatitis C infection: a systematic review of longitudinal studies** *J Viral Hepat* **13**:34–41
5. Santantonio T, Wiegand J, Gerlach JT (2008) **Acute hepatitis C: current status and remaining challenges** *Journal of hepatology* **49**:625–33
6. Fuerst TR, Pierce BG, Keck ZY, Fong SKH (2017) **Designing a B Cell-Based Vaccine against a Highly Variable Hepatitis C Virus** *Front Microbiol* **8**
7. Smith DB, Bukh J, Kuiken C, Muerhoff AS, Rice CM, Stapleton JT, et al. (2014) **Expanded classification of hepatitis C virus into 7 genotypes and 67 subtypes: updated criteria and genotype assignment web resource** *Hepatology* **59**:318–27
8. Hedskog C, Parhy B, Chang S, Zeuzem S, Moreno C, Shafran SD, et al. (2019) **Identification of 19 Novel Hepatitis C Virus Subtypes-Further Expanding HCV Classification** *Open Forum Infect Dis* **6**
9. Li H, Stoddard MB, Wang S, Giorgi EE, Blair LM, Learn GH, et al. (2015) **Single-Genome Sequencing of Hepatitis C Virus in Donor-Recipient Pairs Distinguishes Modes and Models of Virus Transmission and Early Diversification** *Journal of virology* **90**:152–66
10. Bull RA, Luciani F, McElroy K, Gaudieri S, Pham ST, Chopra A, et al. (2011) **Sequential bottlenecks drive viral evolution in early acute hepatitis C virus infection** *PLoS Pathog* **7**
11. Walker MR, Leung P, Eltahla AA, Underwood A, Abayasingam A, Brasher NA, et al. (2019) **Clearance of hepatitis C virus is associated with early and potent but narrowly-directed, Envelope-specific antibodies** *Sci Rep.* **9**
12. Dowd KA, Netski DM, Wang XH, Cox AL, Ray SC (2009) **Selection pressure from neutralizing antibodies drives sequence evolution during acute infection with hepatitis C virus** *Gastroenterology* **136**:2377–86
13. Lavillette D, Tarr AW, Voisset C, Donot P, Bartosch B, Bain C, et al. (2005) **Characterization of host-range and cell entry properties of the major genotypes and subtypes of hepatitis C virus** *Hepatology* **41**:265–74
14. Osburn WO, Snider AE, Wells BL, Latanich R, Bailey JR, Thomas DL, et al. (2014) **Clearance of hepatitis C infection is associated with the early appearance of broad neutralizing antibody responses** *Hepatology* **59**:2140–51

15. Bull RA, Leung P, Gaudieri S, Deshpande P, Cameron B, Walker M, et al. (2015) **Transmitted/Founder Viruses Rapidly Escape from CD8+ T Cell Responses in Acute Hepatitis C Virus Infection** *J Virol* **89**:5478–90
16. Cai C, Samir J, Pirozyan MR, Adikari TN, Gupta M, Leung P, et al. (2022) **Identification of human progenitors of exhausted CD8(+) T cells associated with elevated IFN-gamma response in early phase of viral infection** *Nat Commun* **13**
17. Sanjuan R, Moya A, Elena SF (2004) **The distribution of fitness effects caused by single-nucleotide substitutions in an RNA virus** *Proc Natl Acad Sci U S A* **101**:8396–401
18. Venner CM, Nankya I, Kyeyune F, Demers K, Kwok C, Chen PL, et al. (2016) **Infecting HIV-1 Subtype Predicts Disease Progression in Women of Sub-Saharan Africa** *EBioMedicine* **13**:305–14
19. Zhang H, Bull RA, Quadeer AA, McKay MR (2023) **HCV E1 influences the fitness landscape of E2 and may enhance escape from E2-specific antibodies** *Virus Evol* **9**
20. Quadeer AA, Louie RHY, McKay MR (2019) **Identifying immunologically-vulnerable regions of the HCV E2 glycoprotein and broadly neutralizing antibodies that target them** *Nat Commun* **10**
21. Zhang H, Quadeer AA, McKay MR (2022) **Evolutionary modeling reveals enhanced mutational flexibility of HCV subtype 1b compared with 1a** *iScience* **25**
22. Ferguson AL, Mann JK, Omarjee S, Ndung'u T, Walker BD, Chakraborty AK (2013) **Translating HIV sequences into quantitative fitness landscapes predicts viral vulnerabilities for rational immunogen design** *Immunity* **38**:606–17
23. Barton JP, Goonetilleke N, Butler TC, Walker BD, McMichael AJ, Chakraborty AK (2016) **Relative rate and location of intra-host HIV evolution to evade cellular immunity are predictable** *Nat Commun* **7**
24. Hart GR, Ferguson AL (2015) **Empirical fitness models for hepatitis C virus immunogen design** *Phys Biol* **12**
25. Campo DS, Dimitrova Z, Mitchell RJ, Lara J, Khudyakov Y (2008) **Coordinated evolution of the hepatitis C virus** *Proc Natl Acad Sci U S A* **105**:9685–90
26. Oniangue-Ndza C, Kuntzen T, Kemper M, Berical A, Wang YE, Neumann-Haefelin C, et al. (2011) **Compensatory mutations restore the replication defects caused by cytotoxic T lymphocyte escape mutations in hepatitis C virus polymerase** *J Virol* **85**:11883–90
27. Walker MR, Li H, Teutsch S, Betz-Stablein B, Luciani F, Lloyd AR, et al. (2016) **Incident Hepatitis C Virus Genotype Distribution and Multiple Infection in Australian Prisons** *J Clin Microbiol* **54**:1855–61
28. Kuntzen T, Timm J, Berical A, Lewis-Ximenez LL, Jones A, Nolan B, et al. (2007) **Viral sequence evolution in acute hepatitis C virus infection** *J Virol* **81**:11658–68
29. Kantzanou M, Lucas M, Barnes E, Komatsu H, Dusheiko G, Ward S, et al. (2003) **Viral escape and T cell exhaustion in hepatitis C virus infection analysed using Class I peptide tetramers** *Immunol Lett* **85**:165–71

30. Campo DS, Dimitrova Z, Yamasaki L, Skums P, Lau DT, Vaughan G, et al. (2014) **Next-generation sequencing reveals large connected networks of intra-host HCV variants** *BMC Genomics* **15**
31. Frumento N, Sinnis-Bourozikas A, Paul HT, Stavrakis G, Zahid MN, Wang S, et al. (2024) **Neutralizing antibodies evolve to exploit vulnerable sites in the HCV envelope glycoprotein E2 and mediate spontaneous clearance of infection** *Immunity* **57**:40–51
32. Aurora R, Donlin MJ, Cannon NA, Tavis JE (2009) **Genome-wide hepatitis C virus amino acid covariance networks can predict response to antiviral therapy in humans** *J Clin Invest* **119**:225–36
33. Murray JM, Moenne-Loccoz R, Velay A, Habersetzer F, Doffoel M, Gut JP, et al. (2013) **Genotype 1 hepatitis C virus envelope features that determine antiviral response assessed through optimal covariance networks** *PLoS One* **8**
34. Leung P, Bull R, Lloyd A, Luciani F (2014) **A bioinformatics pipeline for the analyses of viral escape dynamics and host immune responses during an infection** *Biomed Res Int* **2014**
35. Page K, Melia MT, Veenhuis RT, Winter M, Rousseau KE, Massaccesi G, et al. (2021) **Randomized Trial of a Vaccine Regimen to Prevent Chronic HCV Infection** *N Engl J Med* **384**:541–9
36. Cunningham EB, Hajarizadeh B, Bretana NA, Amin J, Betz-Stablein B, Dore GJ, et al. (2017) **Ongoing incident hepatitis C virus infection among people with a history of injecting drug use in an Australian prison setting, 2005-2014: The HITS-p study** *J Viral Hepat.* **24**:733–41
37. White B, Dore GJ, Lloyd AR, Rawlinson WD, Maher L (2014) **Opioid substitution therapy protects against hepatitis C virus acquisition in people who inject drugs: the HITS-c study** *Med J Aust* **201**:326–9
38. Page-Shafer K, Pappalardo BL, Tobler LH, Phelps BH, Edlin BR, Moss AR, et al. (2008) **Testing strategy to identify cases of acute hepatitis C virus (HCV) infection and to project HCV incidence rates** *J Clin Microbiol* **46**:499–506
39. Glynn SA, Wright DJ, Kleinman SH, Hirschhorn D, Tu Y, Heldebrant C, et al. (2005) **Dynamics of viremia in early hepatitis C virus infection** *Transfusion* **45**:994–1002
40. Gaudieri S, Rauch A, Park LP, Freitas E, Herrmann S, Jeffrey G, et al. (2006) **Evidence of viral adaptation to HLA class I-restricted immune pressure in chronic hepatitis C virus infection** *J Virol* **80**:11094–104
41. Bull RA, Eltahla AA, Rodrigo C, Koekkoek SM, Walker M, Pirozyan MR, et al. (2016) **A method for near full-length amplification and sequencing for six hepatitis C virus genotypes** *BMC Genomics* **17**
42. Rodrigo C, Walker MR, Leung P, Eltahla AA, Grebely J, Dore GJ, et al. (2017) **Limited naturally occurring escape in broadly neutralizing antibody epitopes in hepatitis C glycoprotein E2 and constrained sequence usage in acute infection** *Infect Genet Evol* **49**:88–96
43. Zagordi O, Bhattacharya A, Eriksson N, Beerenwinkel N (2011) **ShoRAH: estimating the genetic diversity of a mixed sample from next-generation sequencing data** *BMC Bioinformatics* **12**

44. Wilm A, Aw PP, Bertrand D, Yeo GH, Ong SH, Wong CH, et al. (2012) **LoFreq: a sequence-quality aware, ultra-sensitive variant caller for uncovering cell-population heterogeneity from high-throughput sequencing datasets** *Nucleic Acids Res* **40**:11189–201
45. Topfer A, Zagordi O, Prabhakaran S, Roth V, Halperin E, Beerenwinkel N (2013) **Probabilistic inference of viral quasispecies subject to recombination** *J Comput Biol* **20**:113–23
46. Salazar-Gonzalez JF, Salazar MG, Keele BF, Learn GH, Giorgi EE, Li H, et al. (2009) **Genetic identity, biological phenotype, and evolutionary pathways of transmitted/founder viruses in acute and early HIV-1 infection** *J Exp Med* **206**:1273–89
47. Asquith B, Edwards CT, Lipsitch M, McLean AR (2006) **Inefficient cytotoxic T lymphocyte-mediated killing of HIV-1-infected cells in vivo** *PLoS Biol* **4**
48. Team RCD (2012) **R: a language and environment for statistical computing** Vienna, Austria: R Foundation for Statistical Computing
49. Walker MR, Eltahla AA, Mina MM, Li H, Lloyd AR, Bull RA (2020) **Envelope-specific IgG3 and IgG1 responses are associated with clearance of acute hepatitis C virus infection** *Viruses* **12**
50. Walker MR, Leung P, Eltahla AA, Underwood A, Abayasingam A, Brasher NA, et al. (2019) **Clearance of hepatitis C virus is associated with early and potent but narrowly-directed, Envelope-specific antibodies** *Scientific reports* **9**
51. Wickham H (2016) **ggplot2: Elegant Graphics for Data Analysis** New York: Springer-Verlag

Author information

Melanie R Walker[†]

The Kirby Institute Viral Immunology Systems Program, Faculty of Medicine, The University of New South Wales, Sydney, Australia, School of Biomedical Sciences Viral Immunology Systems Program, Faculty of Medicine, The University of New South Wales, Sydney, Australia
ORCID iD: [0000-0002-9731-9880](https://orcid.org/0000-0002-9731-9880)

[†]These authors contributed equally.

Preston Leung[†]

The Kirby Institute Viral Immunology Systems Program, Faculty of Medicine, The University of New South Wales, Sydney, Australia

[†]These authors contributed equally.

Elizabeth Keoshkerian

The Kirby Institute Viral Immunology Systems Program, Faculty of Medicine, The University of New South Wales, Sydney, Australia, School of Biomedical Sciences Viral Immunology Systems Program, Faculty of Medicine, The University of New South Wales, Sydney, Australia

Mehdi R Pirozyan

The Kirby Institute Viral Immunology Systems Program, Faculty of Medicine, The University of New South Wales, Sydney, Australia, School of Biomedical Sciences Viral Immunology Systems Program, Faculty of Medicine, The University of New South Wales, Sydney, Australia

Andrew R Lloyd

School of Biomedical Sciences Viral Immunology Systems Program, Faculty of Medicine, The University of New South Wales, Sydney, Australia

Fabio Luciani[^]

School of Biomedical Sciences Viral Immunology Systems Program, Faculty of Medicine, The University of New South Wales, Sydney, Australia

For correspondence: luciani@unsw.edu.au

[^]These authors contributed equally.

Rowena A Bull[^]

The Kirby Institute Viral Immunology Systems Program, Faculty of Medicine, The University of New South Wales, Sydney, Australia, School of Biomedical Sciences Viral Immunology Systems Program, Faculty of Medicine, The University of New South Wales, Sydney, Australia

For correspondence: r.bull@unsw.edu.au

[^]These authors contributed equally.

Editors

Reviewing Editor

Laura Delgui

National Scientific and Technical Research Council, Mendoza, Argentina

Senior Editor

Betty Diamond

The Feinstein Institute for Medical Research, Manhasset, United States of America

Reviewer #1 (Public review):

Summary:

The authors examine CD8 T cell selective pressure in early HCV infection using. They propose that after initial CD8-T mediated loss of virus fitness, in some participants around 3 months after infection, HCV acquires compensatory mutations and improved fitness leading to virus progression.

Strengths:

Throughout the paper, the authors apply well-established approaches in studies of acute to chronic HIV infection for studies of HCV infection. This lends rigor to the authors' work.

Weaknesses:

(1) The Discussion could be strengthened by a direct discussion of the parallels/differences in results between HIV and HCV infections in terms of T cell selection, entropy, and fitness.

- (2) In the Results, please describe the Barton model functionality and why the fitness landscape model was most applicable for studies of HCV viral diversity.
- (3) Recognize the caveats of the HCV mapping data presented.
- (4) The authors should provide more data or cite publications to support the authors' statement that HCV-specific CD8 T cell responses decline following infection.
- (5) Similarly, as the authors' measurements of HCV T and humoral responses were not exhaustive, the text describing the decline of T cells with the onset of humoral immunity needs caveats or more rigorous discussion with citations (Discussion lines 319-321).
- (6) What role does antigen drive play in these data -for both T can and antibody induction?
- (7) Figure 3 - are the X and Y axes wrongly labelled? The Divergent ranges of population fitness do not make sense.
- (8) Figure S3 - is the green line, average virus fitness?
- (9) Use the term antibody epitopes, not B cell epitopes.

<https://doi.org/10.7554/eLife.102232.1.sa1>

Reviewer #2 (Public review):

Summary:

In this work, Walker and collaborators study the evolution of hepatitis C virus (HCV) in a cohort of 14 subjects with recent HCV infections. They focus in particular on the interplay between HCV and the immune system, including the accumulation of mutations in CD8+ T cell epitopes to evade immunity. Using a computational method to estimate the fitness effects of HCV mutations, they find that viral fitness declines as the virus mutates to escape T-cell responses. In long-term infections, they found that viral fitness can rebound later in infection as HCV accumulates additional mutations.

Strengths:

This work is especially interesting for several reasons. Individuals who developed chronic infections were followed over fairly long times and, in most cases, samples of the viral population were obtained frequently. At the same time, the authors also measured CD8+ T cell and antibody responses to infection. The analysis of HCV evolution focused not only on variation within particular CD8+ T cell epitopes but also on the surrounding proteins. Overall, this work is notable for integrating information about HCV sequence evolution, host immune responses, and computational metrics of fitness and sequence variation. The evidence presented by the authors supports the main conclusions of the paper described above.

Weaknesses:

One notable weakness of the present version of the manuscript is a lack of clarity in the description of the method of fitness estimation. In the previous studies of HIV and HCV cited by the authors, fitness models were derived by fitting the model (equation between lines 435 and 436) to viral sequence data collected from many different individuals. In the section "Estimating survival fitness of viral variants," it is not entirely clear if Walker and collaborators have used the same approach (i.e., fitting the model to viral sequences from many individuals), or whether they have used the sequence data from each individual to

produce models that are specific to each subject. If it is the former, then the authors should describe where these sequences were obtained and the statistics of the data.

If the fitness models were inferred based on the data from each subject, then more explanation is needed. In prior work, the use of these models to estimate fitness was justified by arguing that sequence variants common to many individuals are likely to be well-tolerated by the virus, while ones that are rare are likely to have high fitness costs. This justification is less clear for sequence variation within a single individual, where the viral population has had much less time to "explore" the sequence landscape. Nonetheless, there is precedent for this kind of analysis (see, e.g., Asti et al., PLoS Comput Biol 2016). If the authors took this approach, then this point should be discussed clearly and contrasted with the prior HIV and HCV studies.

Another important point for clarification is the definition of fitness. In the abstract, the authors note that multiple studies have shown that viral escape variants can have reduced fitness, "diminishing the survival of the viral strain within the host, and the capacity of the variant to survive future transmission events." It would be helpful to distinguish between this notion of fitness, which has sometimes been referred to as "intrinsic fitness," and a definition of fitness that describes the success of different viral strains within a particular individual, including the potential benefits of immune escape. In many cases, escape variants displace variants without escape mutations, showing that their ability to survive and replicate within a specific host is actually improved relative to variants without escape mutations. However, escape mutations may harm the virus's ability to replicate in other contexts. Given the major role that fitness plays in this paper, it would be helpful for readers to clearly discuss how fitness is defined and to distinguish between fitness within and between hosts (potentially also mentioning relevant concepts such as "transmission fitness," i.e., the relative ability of a particular variant to establish new infections).

One concern about the analysis is in the test of Shannon entropy as a way to quantify the rate of escape. The authors describe computing the entropy at multiple time points preceding the time when escape mutations were observed to fix in a particular epitope. Which entropy values were used to compare with the escape rate? If just the time point directly preceding the fixation of escape mutations, could escape mutations have already been present in the population at that time, increasing the entropy and thus drawing an association with the rate of escape? It would also be helpful for readers to include a definition of entropy in the methods, in addition to a reference to prior work. For example, it is not clear what is being averaged when "average SE" is described.

<https://doi.org/10.7554/eLife.102232.1.sa0>